Quaternary Research 72 (2009) 421–430

Contents lists available at ScienceDirect

Quaternary Research

journal homepage: www.elsevier.com/locate/yqres

Luminescence-dated aeolian deposits of late Quaternary age in the southern Tibetan Plateau and their implications for landscape history

ZhongPing Lai [a,c,*], Knut Kaiser [b,c], Helmut Brückner [c]

[a] Luminescence Dating Group, Key Laboratory of Salt Lake Resources and Chemistry, Qinghai Institute of Salt Lakes, Chinese Academy of Sciences, Xining 810008, China
[b] German Academy of Science and Engineering, D-14473 Potsdam, Germany
[c] Faculty of Geography, University of Marburg, D-35032 Marburg, Germany

ARTICLE INFO

Article history:
Received 12 December 2007
Available online 18 August 2009

Keywords:
Aeolian deposits
Quartz luminescence dating
Palaeoenvironmental change
Tibetan Plateau

ABSTRACT

Aeolian deposits are widely distributed in the interior of the Tibetan Plateau, and their chronology is poorly known. It is not yet clear whether they accumulated only after the last deglaciation, or over a longer time. We applied quartz OSL dating to aeolian samples from the Lhasa area with OSL ages ranging from 2.9 ± 0.2 to at least 118 ± 11 ka. The probability density frequency (PDF) distribution of 24 ages reveals age clusters at about 3, 8, 16–21, 33, and 79–83 ka, indicating enhanced sediment accumulation then. The results show that aeolian deposition occurred throughout most of the last 100 ka. This implies that: 1) an ice sheet covering the whole Tibetan Plateau during the last glacial maximum (LGM) could not have existed; and 2) erosion during the last deglaciation was not as strong as previously proposed, such that not all pre-Holocene loess was removed. The age distribution shown in the PDF indicates that aeolian accumulation is episodic. Sand-formation events revealed by age clusters at 3, 8, and 16–21 ka imply roughly synchronous environmental responses to corresponding global-scale arid events.

Introduction

The Tibetan Plateau occupies an area of c. 2.2 million km^2 and has an average elevation of ~5000 m above sea level (asl) (Fielding et al., 1994). The extent of glaciations on the Tibetan Plateau is controversial. Kuhle (e.g. 1998, 2005) proposed that there was an ice sheet of 2.4 million km^2 in area, 2 to 2.5 km thick, covering nearly the whole Tibetan Plateau during different Pleistocene glaciations. However, increasing evidence suggests that glaciations on the Tibetan Plateau were restricted and characterized by valley glaciers or small mountain glaciers (e.g. Derbyshire et al., 1991; Shi et al., 1992; Zheng and Rutter, 1998; Zhou and Li, 1998; Lehmkuhl et al., 2000; Owen et al., 2002). These different views lead to different interpretations of the impact of Tibetan glaciations on global palaeoclimatic changes.

The Tibetan Plateau also plays an important role in both regional and global climatic systems today (Ye and Gao, 1988; Böhner, 1994). In winter, the westerlies are divided into north and south branches at the west end of the Tibetan Plateau, and then converge at the east edge. The north branch of the westerlies is largely responsible for the lower-level formation of several anticyclones in the Asian inland, such as the Siberian-Mongolian High. During summer, air temperature in the Plateau rises above the zonal mean for the free atmosphere at the same elevation, which intensifies the pressure gradient, and thus strengthens the South Asian summer monsoon (Ye and Gao, 1988). The onset and evolution of the Indian and East Asian monsoons have been linked to the uplift phases of the Tibetan Plateau (Ruddimann and Kutzbach, 1989), which induced the development of loess-palaeosol sequences on the Chinese Loess Plateau (An et al., 2001). These sequences have been regarded as sensitive paleoenvironmental indicators.

In the interior Tibetan Plateau with an average elevation of >3500 m asl, long-term and continuous paleoenvironmental records have been obtained mainly from ice cores (Thompson et al., 1989, 1997; Yao et al., 1997) and lacustrine sediments (e.g. Gasse et al., 1996; Herzschuh et al., 2006; Wu et al., 2006). However, it is difficult and expensive to drill ice cores, and most of the lakes in the interior Tibetan Plateau have accumulated sediments only since the late glacial period, whereas the access to loess and aeolian sand is more convenient. Under favorable circumstances, aeolian sediments in the Tibetan Plateau can provide continuous paleoenvironmental information since the last interglaciation (e.g. Fang et al., 2003; Lu et al., 2004). Although loess-palaeosol sequences on the Chinese Loess Plateau have been intensively studied as sensitive palaeoclimatic recorders (e.g. Liu, 1985; Kukla and An, 1989; An et al., 1991; Ding et al., 1992; Porter and An, 1995; Lai and Wintle, 2006), loess deposition on the adjacent Tibetan Plateau has attracted only limited attention.

Aeolian deposits on the Tibetan Plateau are partly associated with glacial activity. In areas where the surface was glaciated during the last glaciation (see Table 1 for its age range), aeolian sediments could accumulate only after the last deglaciation. In periglacial areas, the

* Corresponding author.
E-mail addresses: zplai@isl.ac.cn, zplai@yahoo.com.cn (Z. Lai), knut.kaiser@gmx.net (K. Kaiser), h.brueckner@staff.uni-marburg.de (H. Brückner).

0033-5894/$ – see front matter © 2009 University of Washington. Published by Elsevier Inc. All rights reserved.
doi:10.1016/j.yqres.2009.07.005

Table 1
Terms and age ranges for marine oxygen isotope stages (MIS) (age ranges are from Martinson et al., 1987).

	Marine oxygen isotope stage (MIS)	Age range (ka)
Holocene	1	12.1–present
Last glacial maximum (LGM)	2	24.1–12.1
	3	59.0–24.1
	4	73.9–59.0
Last interglaciation	5	129.8–73.9

previously accumulated sediments might have been eroded and sediments might accumulate again (Sun et al., 2007).

Different views exist on the process of loess formation in the interior Tibetan Plateau. Based on geochemical, mineralogical, and granulometrical evidence, Sun et al. (2007) demonstrated that—unlike the loess on the Chinese Loess Plateau where the dust source was from distant deserts—loess deposits in their study area along the middle reaches of the Yarlung Zangbo River were locally derived during the last glaciation. Then, glaciers expanded and the production of silt-sized particles was increased. Silt particles were deflated from braided river channels by local near-surface winds. Fang (1995) argued that, for loess in the eastern edge of the Tibetan Plateau, dust comes mainly from central and western Tibetan Plateau through transport by the high-level westerlies and the Tibetan winter monsoon. According to Lehmkuhl et al. (2000), for loess in the higher mountain areas of eastern Tibet as well as in western Tibet, coarser grains appear to derive from local materials, silts may represent the long-distance dust flux.

In an ice core from the Guliya ice cap in the Tibetan Plateau, the average concentration of dust (0.63–50.0 μm diameter) during the last glaciation was 6% higher than during the Holocene and 37% higher than during the last interglaciation (Thompson et al., 1997). This implies that dust has been available on the Tibetan Plateau since the last interglaciation, and that loess deposition might have reached its maximum thickness during the last glaciation. However, based on OSL dating of samples from middle reaches of the Yarlung Zangbo river in southern Tibet and the analysis of some previously published dating results, Sun et al. (2007) concluded that present loess deposits in the interior of Tibet accumulated after the last deglaciation and had a basal age of 13–11 ka. According to these authors, the lack of full-glacial loess deposition is either due to the minimal vegetation cover with resultant limited dust-retention ability, or due to erosion of loess as glaciofluvial outwash during the beginning of each interglaciation period, and not due to the lack of silt availability. They also noted that

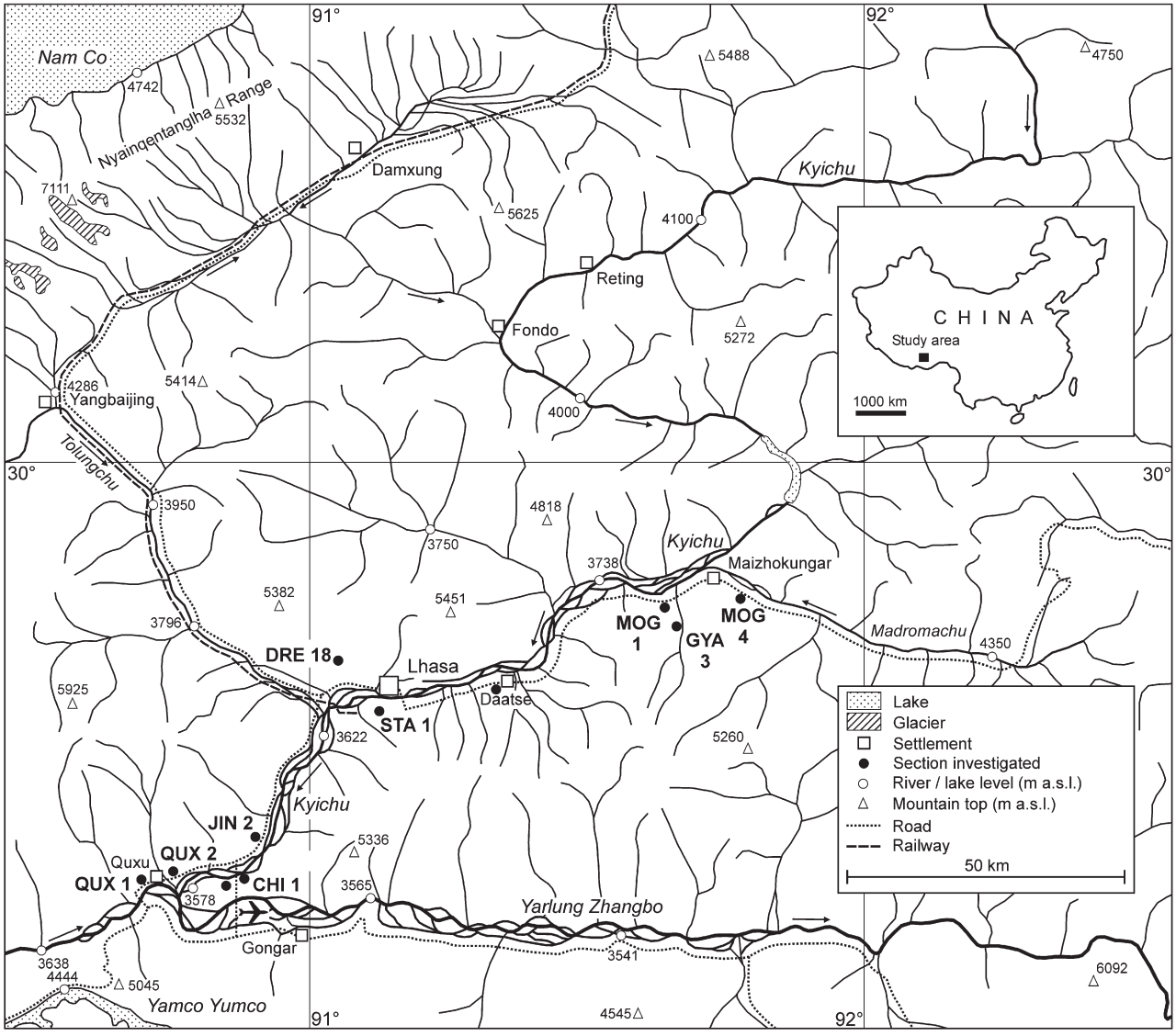

Figure 1. Map showing the study area and the sections investigated.

https://doi.org/10.1016/j.yqres.2009.07.005 Published online by Cambridge University Press

within their study area loess occurs mainly between 3800 and 4300 m asl, where steppe vegetation had effectively trapped aeolian silts. With respect to the distribution of loess and loess-like sediments within the Tibetan Plateau, Lehmkuhl (1997) and Lehmkuhl et al. (2000) argued that in general Holocene loess lies above ~4000 m asl, whereas Pleistocene loess lies below ~4000 m asl. These authors also reported (a) that up to several meters of typical loess occurs in basins of eastern Tibet below 3600 m asl, and (b) that in areas above ~3600 m asl and up to 4300 m asl in eastern Tibet and up to more than 5000 m asl in western Tibet, this aeolian cover is dominated by sandy loess.

Numerical chronologies for aeolian deposits in the interior Tibetan Plateau are still limited. Although the majority of luminescence and radiocarbon dating results indicate that aeolian sediments in the Tibetan Plateau accumulated during the Holocene (Péwé et al., 1995; Lehmkuhl et al., 2000; Porter et al., 2001; Li et al., 2006; Owen et al., 2006; Sun et al., 2007), some results suggest that the aeolian sediments could date back to the last glaciation (Lehmkuhl et al., 2002; Kaiser, 2007).

In the present study, in order to expand our knowledge of chronology of aeolian deposits in the interior Tibetan Plateau, nine aeolian sections in the Lhasa area, southern Tibet, were investigated using optically stimulated luminescence (OSL) of quartz, as a part of a research project investigating the late Quaternary landscape evolution of the Kyichu river catchment (Kaiser et al., 2009a,b,c,d; Fig. 1).

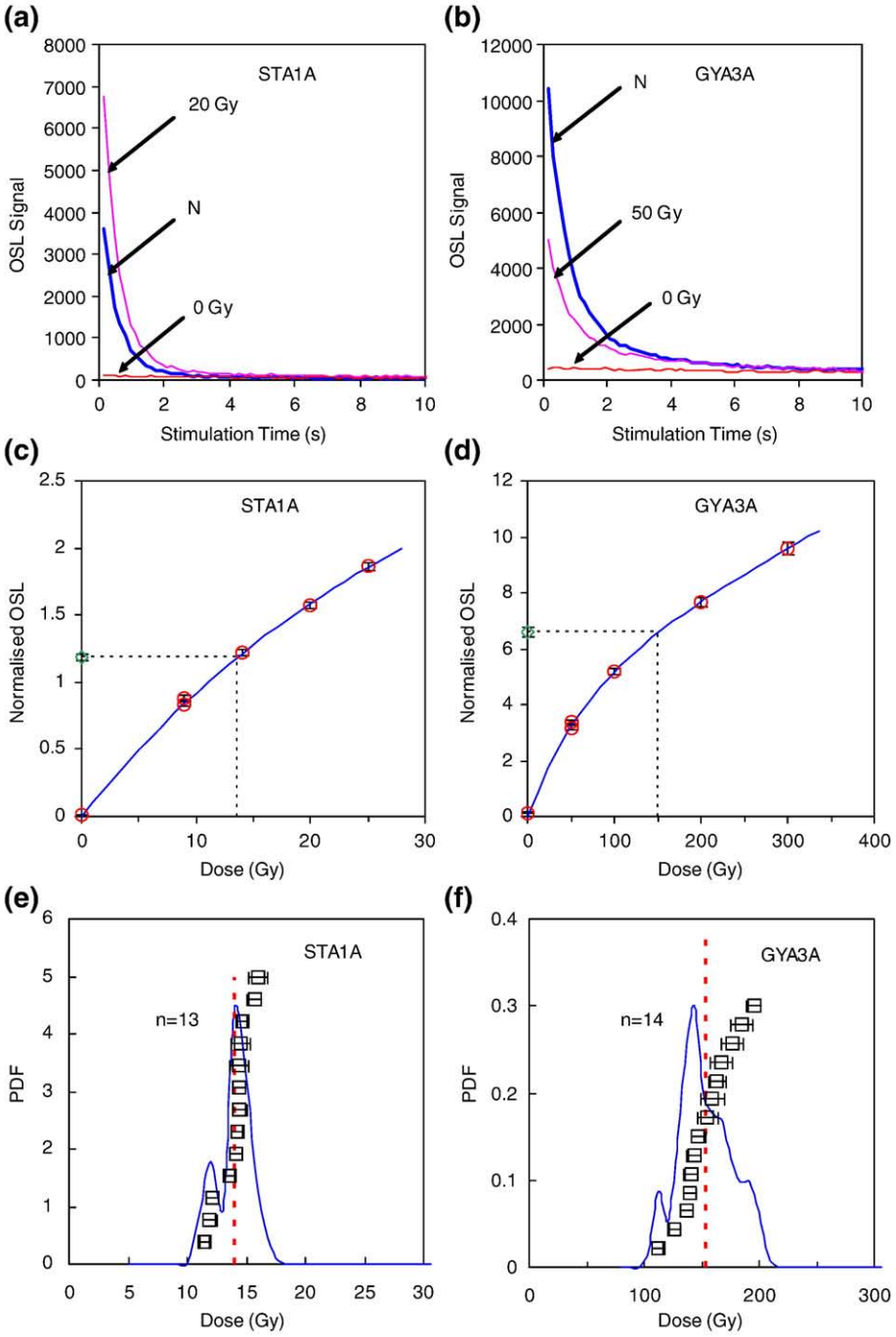

Figure 2. OSL characteristics (shine-down curves, growth curves, and D_e distributions) for an aeolian sand sample STA1A (left column) and a loess sample GYA3A (right column). The vertical dotted lines in (e) and (f) show the mean equivalent doses for the two samples, respectively.

https://doi.org/10.1016/j.yqres.2009.07.005 Published online by Cambridge University Press

Study area and luminescence samples

Selected sites under study are located in the Kyichu river valley and its tributaries (Fig. 1). The area belongs to the catchment of the Yarlung Zangbo River, and is covered by a thin veneer (<1 m) of aeolian sediments, except for active fluvial and peat bog sites, screes or barren rocks. In the middle and lower Kyichu river valley there are some larger basins, such as the Lhasa Basin (~3650 m asl), the north–south dimension of which reaches ~6 km. Larger areas of active aeolian sediments exist on valley flanks in the river mouth area adjoining the Yarlung Zangbo river (Atlas of Tibet Plateau, 1990). In Lhasa (~3650 m asl), the mean annual temperature (MAT) is 7.7°C, with summer temperatures of >15.5°C and winter temperatures below −2.1°C (Domrös and Peng, 1988; Miehe et al., 2001). The mean annual precipitation (MAP) in the study area is 361–490 mm. This area is dominated by the southwest Asian monsoon.

Nine sections (Figs. 1 and 3) were selected and a total of twenty-seven samples for luminescence dating were collected. These included twenty-four aeolian sediment samples, one sample each from lacustrine and fluvial sand, and one surface sample (CHI1G) collected from section CHI1 for checking luminescence clock-zeroing assumption (by daylight exposure). Samples were collected by driving iron tubes (~18 cm in length and ~5–6 cm in diameter) into the freshly prepared section. The ends of each tube were covered by a thick black cloth when the tube was filled with sediment, and then wrapped with opaque plastic tape.

Sample preparation and measurement techniques

The samples in the iron tubes were sub-sampled under subdued red light. The outer 2–3 cm were removed and the interior were used for further processing that involved, pretreatment with 10% HCl (to remove carbonates), 38% H_2O_2 (to remove organics) and wet sieving for 38–63 μm grain fraction. The fraction of 38–63 μm was etched with 35% hydrofluorosilicic acid (H_2SiF_6) for about 2 weeks to dissolve feldspars and then with 10% HCl to remove any acid-soluble fluoride precipitates. The purity of the extracted quartz was checked by IR (830 nm) stimulation. The quartz grains were then thinly spread on the center part (with a diameter of 5–6 mm) of stainless steel discs (with a diameter of 9 mm) using silicone oil.

The OSL experiment was carried out in the Marburg Luminescence Laboratory, University of Marburg, Germany. Luminescence measurements were performed on a Risø TL-DA-15 reader TL/OSL system (Bøtter-Jensen et al., 2000), equipped with a $^{90}Y/^{90}Sr$ beta source and blue LEDs ($\lambda = 470 \pm 20$ nm) for optical stimulation. Quartz OSL signals were recorded at 130°C for 60 s using a photomultiplier tube with the luminescence filtered through two U-340 glass filters. The concentrations of uranium, thorium, and potassium were measured by Inductively Coupled Plasma Mass Spectrometry (ICP-MS) at Cologne University, Germany. The "a value" for quartz was taken as 0.035 ± 0.003 (Lai et al., 2008a), and the water content $10 \pm 5\%$ for all samples. The cosmic-ray dose rate was estimated according to Prescott and Hutton (1994).

Equivalent dose determination

Because the equivalent dose (D_e) could be severely underestimated for some loess samples when using feldspar infra-red stimulated luminescence (IRSL) (Aitken, 1998; Lai and Brückner, 2008), quartz was selected for D_e determination in the current study. The single-aliquot regenerative-dose (SAR) protocol (Murray and Wintle, 2000) has been shown to be suitable for D_e determination for quartz of medium grain size (e.g. 38–63 μm) extracted from loess (Roberts et al., 2003; Lai and Wintle, 2006; Lai et al., 2007; Lai, in press). For growth curve construction using the SAR protocol, seven regeneration dose points were used. These included a zero-dose for the measurement of recuperation and a recycling ratio (for assessing the sensitivity change correction). At the end of the protocol, the sample was dosed and tested for feldspar contamination.

Laboratory dose (50 Gy) recovery test was performed on sample GYA 3B, with preheat temperatures increasing from 220 to 300°C at an interval of 20°C, and with a test dose of 11 Gy and readout time of 60 s at a temperature of 130°C. For all experiments we used hold times of 10 s for both preheats and cutheats. For each preheat temperature

Table 2
OSL dating results.

Lab. no.	Sample	Depth (cm)	Coordinates	Altitude (m a.s.l.)	Sediment type	U (ppm)	Th (ppm)	K (%)	Dose rate (Gy/ka)	Number of aliquots	Equivalent dose (Gy)	OSL age (ka)
MR0545	STA1A	50	29°37′59.4″N, 91°05′52.0″E	~3660	Aeolian sand	2.76 ± 0.19	17.33 ± 1.21	2.72 ± 0.14	4.76 ± 0.36	13	14 ± 0.4	2.9 ± 0.2
MR0546	STA1B	180			Aeolian sand	2.69 ± 0.18	17.34 ± 1.21	2.68 ± 1.13	4.64 ± 0.36	14	19 ± 1.1	4.1 ± 0.4
MR0547	STA1C	280			Aeolian sand	3.10 ± 0.22	18.73 ± 1.31	2.65 ± 0.13	4.78 ± 0.37	11	32 ± 0.6	6.7 ± 0.5
MR0548	QUX 1A	280	29°21′19.0″N, 90°43′25.1″E	~3603	Aeolian sand	2.15 ± 0.11	15.20 ± 1.06	2.82 ± 0.19	4.00 ± 0.30	11	34 ± 1	8.5 ± 0.7
MR0549	JIN 2A	130	29°25′38.7″N, 90°54′27.3″E	~3597	Aeolian sand[a]	2.68 ± 0.13	13.91 ± 0.97	2.19 ± 0.15	4.28 ± 0.33	12	33 ± 2	7.7 ± 0.8
MR0550	JIN 2B	250			Aeolian sand	2.76 ± 0.14	13.08 ± 0.92	2.04 ± 0.14	4.20 ± 0.33	11	60 ± 5	14.3 ± 1.6
MR0551	JIN 2C	340			Aeolian sand	2.63 ± 0.13	20.4 ± 1.43	3.24 ± 0.23	4.90 ± 0.38	11	92 ± 7	18.8 ± 2.0
MR0552	CHI1F	70	29°21′47.9″N, 90°53′36.0″E	~3820	Aeolian sand	2.66 ± 0.19	18.4 ± 1.29	2.79±0.14	4.86 ± 0.37	12	70 ± 4	14.4 ± 1.4
MR0553	CHI1E	300			Aeolian sand	2.83 ± 0.20	18.3 ± 1.28	2.86 ± 0.14	4.86 ± 0.38	13	96 ± 5	19.8 ± 1.9
MR0554	CHI1C	650			Aeolian sand	2.33 ± 0.16	15.28 ± 1.07	2.45 ± 0.12	4.05 ± 0.32	14	97 ± 4	23.9 ± 2.1
MR0555	CHI1B	1000			Aeolian sand	2.86 ± 0.20	17.21 ± 1.21	2.95 ± 1.15	4.74 ± 0.38	11	101 ± 3	21.3 ± 1.8
MR0556	QUX2A	130	29°21′57.3″N, 90°45′20.2″E	~3536	Aeolian sand	1.92 ± 0.13	11.36 ± 0.79	2.63 ± 0.13	3.97 ± 0.31	14	69 ± 2	17.2 ± 1.4
MR0557	QUX2B	600			Lacustrine silt	2.71 ± 0.19	17.71 ± 1.24	2.67 ± 0.13	4.48 ± 0.34	13	73 ± 7	16.3 ± 2.0
MR0558	QUX2C	950			Fluvial sand	2.74 ± 0.19	15.5 ± 1.08	2.45 ± 0.12	4.09 ± 0.31	17	113 ± 5	27.7 ± 2.5
MR0559	MOG4A	130	29°47′30.0″N, 91°48′45.2″E	~3894	Aeolian sand	3.45 ± 0.24	22.26 ± 1.56	2.33 ± 0.12	4.93 ± 0.37	14	139 ± 11	28.2 ± 3.1
MR0560	MOG4C	350			Aeolian sand	2.99 ± 0.21	18.21 ± 1.28	2.29 ± 0.12	4.39 ± 0.34	13	354 ± 12	81 ± 7
MR0561	MOG4E	600			Loess	3.25 ± 0.23	20.62 ± 1.44	2.48 ± 0.12	4.73 ± 0.37	12	388 ± 19	82 ± 8
MR0562	MOG4F	800			Loess	3.15 ± 0.22	16.76 ± 1.17	2.37 ± 0.12	4.29 ± 0.33	13	506 ± 29	118 ± 11
MR0563	GYA3A	160	29°44′54.6″N, 91°40′02.5″E	~3840	Loess	3.0 ± 0.21	19.46 ± 1.36	2.31 ± 0.12	4.52 ± 0.34	14	154 ± 7	34.1 ± 3.0
MR0564	GYA3B	320			Loess	3.04 ± 0.21	18.58 ± 1.30	2.34 ± 0.12	4.50 ± 0.34	14	202 ± 9	45 ± 4
MR0565	GYA3C	400			Loess	1.92 ± 0.13	11.36 ± 0.80	2.63 ± 0.13	4.45 ± 0.34	12	279 ± 24	63 ± 7
MR0566	DRE18A	330	29°40′09.7″N, 91°02′41.6″E	~3707	Aeolian sand	3.26 ± 0.23	21.00 ± 1.47	2.44 ± 0.12	4.79 ± 0.37	13	155 ± 10	32.3 ± 3.2
MR0567	DRE18B	590			Loess[a]	5.46 ± 0.38	19.55 ± 1.37	1.91 ± 0.09	4.72 ± 0.36	12	326 ± 23	69 ± 7
MR0568	DRE18C	850			Loess[a]	3.59 ± 0.25	21.99 ± 1.54	2.18 ± 0.11	4.61 ± 0.36	14	377 ± 19	82 ± 8
MR0569	MOG 1A	600	29°47′57.0″N, 91°38′06.2″E	~3778	Loess	2.09 ± 0.10	14.66 ± 1.03	2.36 ± 0.16	3.67 ± 0.29	14	289 ± 21	79 ± 8
MR0570	MOG 1B	800			Loess	2.04 ± 0.10	17.08 ± 1.19	2.90 ± 0.20	3.98 ± 0.31	14	410 ± 31	103 ± 11

The water content is taken as 10 ± 5 for all samples.
[a] Has been developed into palaeosol. A modern sample from section CHI1 gave a D_e of 0.37 ± 0.06 Gy.

https://doi.org/10.1016/j.yqres.2009.07.005 Published online by Cambridge University Press

point, four aliquots were used for D_e determination. The average recovered D_e for the four aliquots for each temperature point was from 49.1 ± 0.9 to 52.7 ± 1.5 Gy, and the average recovered D_e for all twenty aliquots (five temperature points and four aliquots for each point) was 50.9 ± 0.5 Gy. The results suggest that the recovered D_e is insensitive to the preheat temperatures used, and that a known laboratory dose can be successfully recovered using our SAR procedures. As a result, the preheat temperature was chosen to be 260°C for 10 s. For all samples, the recuperation value was <0.3% which is minor, and the average recycling ratio was 0.99 ± 0.01, identical within error to the ideal value of 1 (Murray and Wintle, 2000).

Examples of shine-down curves, growth curves and D_e distributions for samples STA1A and GYA3A are shown in Figure 2. It is clear that the OSL signal was dominated by a 'fast component' (e.g. Wintle and Murray, 2006), and OSL signals of the first 0.48 s (after background subtraction using the last 25 channels in the shine-down curve) were integrated for equivalent dose estimation. The growth curve was fitted using a single saturation exponential plus linear function. There is clearly a linear growth part in the growth curve beyond a regeneration dose of 200 Gy (Fig. 2c), which may allow for D_e determination to a higher dose range (Lai et al., 2008b; Lai, in press; Fan et al., in press; Long et al., in press; Ou et al., in press; Sun et al., in press). The mechanism for this linear growth has not yet been fully understood (Wintle and Murray, 2006; Lai, in press). D_e values of these two characteristic samples were plotted using the probability density function (Bøtter-Jensen et al., 2003) (Figs. 2e and f). These distributions have a central mode and an approximate symmetry, so that we chose the mean of each entire distribution for age calculation. For each sample at least eleven aliquots were measured. The D_e and the associated standard error for each sample are listed in Table 2.

To evaluate the extent of bleaching by daylight under the natural regional conditions, a surface sample (CHI1G) was collected from

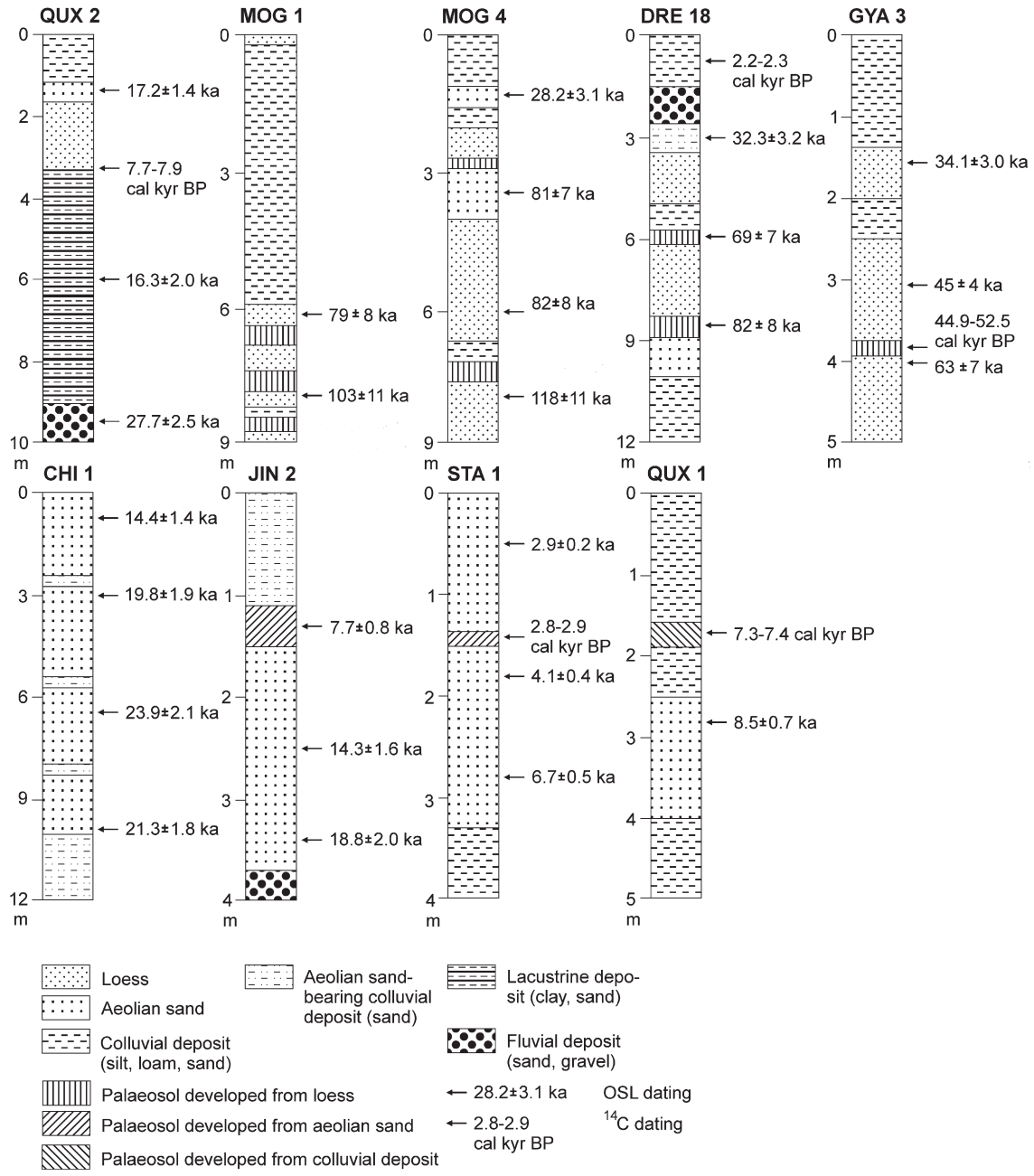

Figure 3. Sediment logs and geochronological data of the sections investigated (radiocarbon ages are quoted from Kaiser et al., 2009a).

https://doi.org/10.1016/j.yqres.2009.07.005 Published online by Cambridge University Press

section CHI1. The D_e for this modern sample is 0.37 ± 0.06 Gy. Assuming that its dose rate is half (receiving irradiation from the sediments below only) of 4.63 Gy/ka, which is the average dose rate for the other four samples from section CHI1, the resultant age for this modern sample is 160 ± 20 years, which is effectively zero compared to the ages for samples in this study. The insignificant D_e value also implies negligible thermal transfer contribution induced by preheat.

Dating results and discussions

Results and its environmental implications

Some OSL/IRSL ages of aeolian sediments from the interior Tibetan Plateau have been published (Lehmkuhl et al., 2000; Porter et al., 2001; Owen et al., 2006; Sun et al., 2007; Madsen et al., 2008; Liu et al., in press). Lehmkuhl et al. (2000) reported OSL ages (using fine-grained quartz) for nine samples from nine sections in central, southern and eastern Tibet. These samples were derived from the base of aeolian sandy silts that lie on top of glacial sediments (moraines) and a terrace. Eight ages are younger than 11 ka (i.e., within the Holocene). One age is 25.5 ± 4.9 ka belonging to the Pleistocene, and this sample was from the aeolian silt mantling the Bomi moraine (with an elevation of about 3000 m asl in southern Tibet). Lehmkuhl et al. (2000) argued that, according to geomorphological investigations, the Bomi moraine should have formed during the last glaciation and that the OSL age confirmed their field observation. The authors also had an additional sample (A023) that was too old to be dated then. However, A. Lang (then at Heidelberg, now at Liverpool) determined an OSL age of more than 85 ka for a sample from the same layer (cited in Lehmkuhl et al., 2000). Using fine grain IRSL, Porter et al. (2001) reported eight ages of regional loess (three loess ages ranging from 45 to 33 ka were excluded in the discussion of this study, as this loess was localized dust accumulation) from Qinghai Lake, all of which were younger than 17 ka. They proposed that the absence of loess of full-glacial age and the presence of a weakly developed palaeosol (dated from 33 ± 3 to 16.9 ± 1.4 ka by fine grain IRSL) just below the loess and on top of the bajada gravel imply a stable, cold land surface in that area during the last glaciation. Sun et al. (2007) dated three loess samples collected from three sections in the middle reaches of the Yarlung Zangbo River; all of these quartz OSL ages were younger than 13 ka. The authors also dated a soil sample producing an age of >70 ka. This sample was collected from the top of a soil layer that is overlain by a thick loess bed. Sun et al. (2007) explained that this sample was composed of re-transported soil and fan sediments because fluvial sands and small gravel-sized clasts occurred within this soil layer, which was not well-bleached before deposition.

Luminescence dating results are summarized in Table 2. OSL ages are inserted in the sections according to their depth in Figure 3, together with five radiocarbon ages cited from Kaiser et al. (2009a). For ^{14}C samples, except for one bulk-soil matter sample in section QUX1, all the other four (from sections QUX2, DRE18, GYA3, and STA1) are from charcoals. In section QUX2, a ^{14}C age of 7710–7850 cal yr BP on charcoal collected from the bottom of the aeolian sediments is much younger than the OSL ages above and below, which might be due to silt infiltration of charred root. In section DRE18, the ^{14}C age (2200–2300 cal yr BP) and the OSL ages are in stratigraphic order; the ^{14}C age is much younger than the OSL age (32.3 ± 3.2 ka), because a hiatus exists between them. For the remaining three ^{14}C ages (from sections GYA3, STA1 and QUX1), they are in agreement with the corresponding OSL ages (Fig. 4), and the ratio of ^{14}C ages to OSL ages is 1.04, close to unity. In general, the available radiocarbon ages support the luminescence results.

The 24 luminescence ages from aeolian samples range from 2.9 ± 0.2 to at least 118 ± 11 ka, and suggest that aeolian sediment deposition

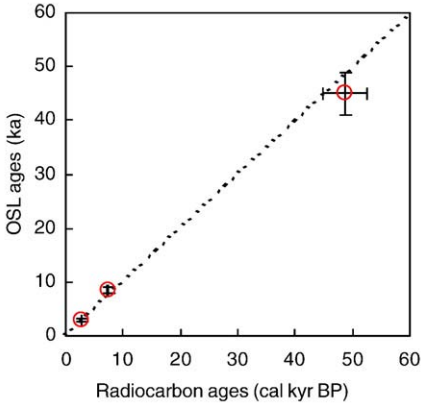

Figure 4. Comparison of OSL ages with ^{14}C ages.

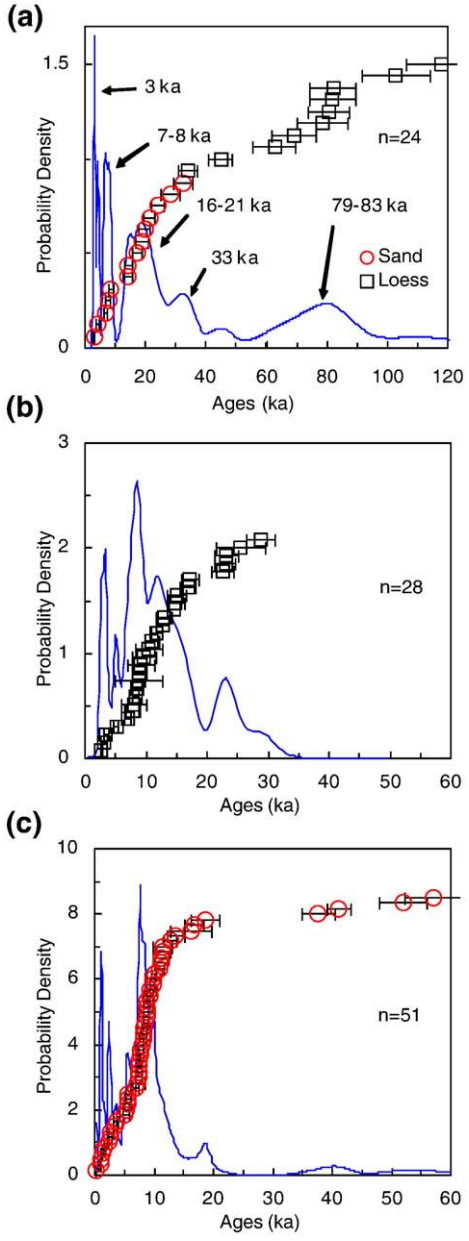

Figure 5. Probability density plot for (a) 24 OSL ages on aeolian samples in this study; (b) previous OSL and IRSL ages ($n = 28$) for aeolian samples from the Tibetan Plateau; and (c) the OSL and IRSL ages ($n = 51$) for sand samples from the Mu Us desert. Details of the ages in (b) and (c) are listed in Supplement Table.

https://doi.org/10.1016/j.yqres.2009.07.005 Published online by Cambridge University Press

occurred from the last interglaciation until the late Holocene. The seven luminescence ages of >69 ka (mainly on loess samples from sections MOG1, MOG4 and DRE18, with D_es>300 Gy) could be treated as minimum ages, as previous studies showed that quartz OSL might saturate at about 200 Gy (Wintle and Murray, 2006). However, the growth curve here (Fig. 2d) did not show saturation till at least 300 Gy, and these age estimates are still in stratigraphic order. These ages imply that the associated sediments accumulated during the last interglaciation. Paleosols in the lower part of sections MOG1, MOG4 and DRE18 support this argument, since it is likely that during the last interglaciation pedogenic processes were active (Kaiser et al., 2009a). In section GYA3, the palaeosol might have been formed during the marine oxygen isotope stage (MIS) 3 between 63.0 ± 7.0 and 44.8 ± 4 ka. For sections QUX2, CHI1, JIN2, STA1 and QUX1, the OSL ages range from 23.9 ± 2.1 to 2.9 ± 0.2 ka, which could mean that the aeolian sediment accumulation occurred from the LGM until the late Holocene.

In order to extract paleoenvironmental information from the distribution of an array of OSL ages, all 24 OSL ages of aeolian samples dated in the current study were plotted using a probability density function (PDF) (Fig. 5), which has been employed for luminescence age distribution analysis (e.g. Singhvi et al., 2001; Telfer and Thomas, 2007). This approach permits the construction of a histogram such that the experimental errors are also included (Singhvi et al., 2001). There is a possibility that the overall distribution of OSL ages in the PDF plot might reflect the sampling strategies rather than the full distribution of ages of preserved aeolian deposits (Telfer and Thomas, 2007). An age cluster in a PDF plot could be interpreted either as a higher and accidental sampling density of sediments belonging to a specific interval and/or as a reflection of an enhanced accumulation (Singhvi et al., 2001). It was suggested that undertaking a greater density of sampling in a systematic manner would minimize this effect, and that it would be further reduced by sampling at frequent and regular intervals (Telfer and Thomas, 2007). In the current study, 21 (out of 24) OSL aeolian samples were collected in roughly regular intervals from sections MOG4, DER18, GYA3, CHI1, JIN2 and STA1 (see Fig. 3). As a result, the distribution of these OSL ages in the PDF plot in Figure 5a reveals the distribution of ages of preserved aeolian deposits, and can provide significant information for the interpretation of aeolian sediment accumulation. The distribution reveals age clusters at 3, 7–8, 16–21, 33, and 79–83 ka, which can be interpreted as enhanced aeolian sediment accumulation during those time periods. It is interesting to note that sand accumulation occurred mainly during the period of 2–30 ka, while loess ages are older than 30 ka (Fig. 5a), whose reason is unknown yet. Even if there is an age cluster at about 79–83 ka, it is not appropriate to conclude that loess accumulation was enhanced in the late part of MIS 5 only, as these OSL ages are close to the saturation limit for quartz OSL dating and their actual ages may be older. But it is most probable that loess deposition existed during the last interglaciation.

A sand accumulation phase in deserts is generally interpreted as representative of an arid period. In Figure 5a, age clusters of sand samples at 3 and 7–8 ka may reflect the global trend of increased aridity in both periods, as the Tibetan Plateau is very sensitive to global changes. Worldwide evidence showed arid events at ca. 3 ka (Wanner et al., 2008, and references therein) and 8 ka (the "8 k event", Alley and Ágústsdóttir, 2005, and reference therein). The mechanism for the arid event at 3 ka is still not clear (Alley and Ágústsdóttir, 2005). Among several century-scale arid events in the Holocene detected using lake sediments from tropical Africa, Central America and west Asia, the arid event at 3 ka was possibly triggered by temporary weakening of the monsoonal circulation associated with the reduced northward heat transport by the oceans or by feedback processes stimulated by changes in tropical land surface conditions (Lamb et al., 1995). It was also proposed that a solar forcing mechanism might underlie the centennial to millennial time-scale changes in the Holocene (detected in sediments from the North Atlantic), and that the surface hydrographic changes might have affected the production of the North Atlantic Deep Water, potentially providing an additional mechanism for amplifying the solar signals and transmitting them globally (Bond et al., 2001). The 8 k event, which brought generally cold and dry conditions to broad northern-hemisphere regions, was in response to a very large outburst flood from ice-dammed lakes in northern America that freshened the North Atlantic (Alley and Ágústsdóttir, 2005). This event has been detected within the Tibetan Plateau (van Campo and Gasse, 1993; Liu et al., 2002). Sand-accumulation events recorded in the Tibetan Plateau at about 3 and 8 ka imply roughly synchronous global climate changes then. In Figure 5a, within the Holocene there are two obvious periods of sand formation quiescence at about 5 and 10 ka (Fig. 5a), implying warm and humid climate conditions or absence of sand sources during both intervals.

In addition to the accumulation within the Holocene, which had also been reported previously (Lehmkuhl et al., 2000; Sun et al., 2007), it is clear that aeolian deposition occurred in the last glaciation, and also during the last interglaciation. A prominent age cluster at about 16–21 ka indicates enhanced sand dune formation during the LGM, which is the most arid period during the last 100 ka. Age clusters at about 33 and 80 ka were also observed. Existence of aeolian deposits during the last 100 ka implies that an ice sheet covering the whole Tibetan Plateau during the LGM (19–23 ka; Kuhle, 1998, 2005) cannot have existed, otherwise the aeolian deposits in the valley older than LGM would have been completely destroyed by this glaciation. Another implication is that the erosion in the investigated area during the last deglaciation was not as strong as in the middle reaches of the Yarlung Zangbo River examined by Sun et al. (2007), who suggested that all loess already deposited had been eroded during the deglaciation and that the loess basal age was less than about 13 ka in the Tibetan Plateau.

However, it should be kept in mind that it is still debated, to some extent, whether ages of dune sands represent an event of aridity or not. For example, Nanson et al. (1992) suggested that the dune field would record only the latter phases of deposition, while the earlier phases were unlikely to be recorded. McFarlane et al. (2005) suggested that linear dune ages in Botswana might not represent the dune-building event at all, but the wetter phases of downslope redistribution of aeolian materials. Accentuated aeolian aggradations will occur during specific climatic regimes, whose timing will then be determined by an optimal combination of sediment supply, transport and preservation or erosion (Singhvi and Porat, 2008). In some cases it is likely to date multiple events in the history of the same sample (Singhvi et al., 1989). As a result, the meaning and implication of a luminescence age of drylands should be carefully examined before presenting interpretation for environmental changes (Singhvi and Porat, 2008; Lancaster, 2008). In any case, this issue is beyond the scope of the current study.

Comparison of age distribution with previously published OSL and IRSL ages in the Tibetan Plateau

It is interesting to compare the distribution of OSL ages in this study to previously published OSL/IRSL ages of aeolian samples from the interior Tibetan Plateau (Lehmkuhl et al., 2000, 11 OSL ages from eastern Tibetan Plateau; Porter et al., 2001, 9 IRSL ages from Qinghai Lake in the northeastern plateau; Owen et al., 2006, 2 OSL ages from the northern plateau; Sun et al., 2007, 3 OSL ages from the southern plateau; Madsen et al., 2008, 1 OSL age from Qinghai Lake in the northeastern plateau; Liu et al., in press, 2 OSL ages from Qinghai Lake in the northeastern plateau). All these previously published OSL/IRSL ages ($n=28$) of aeolian samples (24 of loess and 4 of sand) are collected in Supplement Table and plotted in Figure 5b. Age clusters were observed at 3, 5, 8–9, 11.5–12.5, and 22–24 ka. The main clusters at 3, 8–9, and 22–24 ka are identical to the age distribution in Figure

https://doi.org/10.1016/j.yqres.2009.07.005 Published online by Cambridge University Press

5a. This similarity in age distribution pattern suggests the synchronous aeolian deposit accumulation throughout the whole Tibetan Plateau, regardless of different atmospheric systems dominating different parts of the Tibetan Plateau: the East Asian monsoon dominates in the eastern Tibetan Plateau, the Southwest Asian monsoon in the southern and the westerlies in the northern (Bryson, 1986). Thus, since the LGM the aeolian accumulation events in the Tibetan Plateau reflect synchronous global climate changes transmitted to the Tibetan Plateau through different atmospheric systems. Records from Qinghai Lake in NE Tibetan Plateau also confirmed the rapid climate response to a global-scale driving force during late MIS 2 and the early Holocene (Liu et al., 2002; Shen et al., 2005). A similar observation was also made from ^{14}C chronology of Holocene deposits (mainly lacustrine and paleosols) in the arid to semi-arid transition zone of north-central China (Porter and Zhou, 2006). They demonstrated that East Asian monsoon variations correlate closely with variations in North Atlantic drift-ice tracers that represent episodic advection of drift ice and cold polar surface water southward and eastward into warmer subpolar water, and that the correspondence of these records over the full span of Holocene time implies a close relationship between North Atlantic climate and the monsoon climate of central China.

Comparison of age distribution with published OSL and IRSL ages in the Mu Us desert in northern China

The Mu Us desert is in northern China, mostly in the Inner Mongolia Province. It is located at the present northern limit of East Asian monsoon rainfall, and is therefore sensitive to global climate changes. Recently, a number of OSL dating studies have been conducted in the Mu Us desert (Lai et al., 1999, 2 IRSL ages; Li et al., 2002, 6 OSL ages; Lu et al., 2005, 27 OSL ages; Sun et al., 2006, 17 OSL ages). All these OSL ages ($n = 51$) have been collected in the Supplement Table and plotted in Figure 5c. Five age clusters are evident, at 1, 2.4, 5.5, 7.5–8.5, and 19 ka, with main clusters at 1 and 7.5–8.5 ka. The 7.5–8.5 ka peak is dominant in Figures 5a–c. It suggests a common driving force and synchronous nature for this arid event in both the Tibetan Plateau and the Mu Us desert, which is in agreement with the conclusions by Wang et al. (2008) that the millennial-scale climate events of high-resolution speleothem records in China are synchronous with summer insolation at 65° N (Berger, 1978). Pollen records from Qinghai Lake in NE Tibetan Plateau showed that within the Holocene period the largest amplitude of cold events occurred ca. 8200 years ago (Liu et al., 2002).

The age clusters at 1, 2.4, and 5.5 ka should be associated with human activity. The age cluster at 5.5 ka might be related to the initial stage of agricultural activities in China which occurred in the southeastern margin of the Mu Us desert during that time. The spatial distribution of archaeological sites of the ruins of Late Yangshao Culture (ca. 5.5–5 ka) and the Longshan Culture (ca. 5–4 ka) are distributed in the southeastern margin of the Mu Us desert (Sun et al., 2006). The age cluster at 2.4 ka might be associated with intensive agricultural land use which started during the West Han Period (206 B.C.–A.D. 25), and the 1 ka cluster related to farming economies of the Tang Dynasty (A.D. 618–907). There is a possibility that the peak at 3 ka in Figures 5a and b might also be associated with human activity in the Lhasa area, as it was the human impact that destroyed the natural forest in the Lhasa area some time during the last 5000 years (Miehe et al., 2006; Kaiser et al., 2009a,b). The detection of centennial-scale events of human impact on the landscape history in the Mu Us desert within the last ca. 5 ka indicated that the PDF plot is a powerful tool for the analysis of OSL ages and its implications for environmental changes. The pattern of age distribution in Figure 5 shows that the accumulation and preservation of aeolian dust is, in general, episodic, as has been demonstrated elsewhere for drylands (e.g. Singhvi et al., 2001; Lancaster, 1990, 2008).

Conclusions

Twenty-seven samples (24 aeolian, 1 lacustrine, 1 fluvial, and 1 surface sample) from nine sections in the Lhasa area on the Tibetan Plateau were dated using OSL of silt-sized quartz (38–63 μm). Where ^{14}C ages are available, the OSL ages are in general agreement with them. Ages of aeolian sediments range from 2.9 ± 0.2 to at least 118 ± 11 ka. When all the ages of aeolian sediments were plotted using a probability density function, the distribution reveals age clusters at 3, 7–8, 16–21, 33, 45, and 79–83 ka, which could be interpreted as a reflection of an enhanced sediment accumulation during those time periods.

In addition to the accumulation within the Holocene, aeolian deposition occurred in the last glaciation, and also within the last interglaciation. The dating results support the view that an ice sheet covering the whole Tibetan Plateau during the LGM did not exist, and that the erosion during the last deglaciation was not as strong as previously thought that it might have removed all loess deposition accumulated before the Holocene.

The pattern of age distribution in a PDF plot showed that aeolian dust accumulation/preservation is in general episodic in the interior Tibetan Plateau. The main age clusters in the PDF plot at 3, 8, and 16–21 ka in Figure 5a (data from Lhasa area only) are identical to those in Figure 5b (data from different parts of the Tibetan Plateau). This similarity suggests synchronous aeolian deposit accumulation throughout the whole Tibetan Plateau, regardless of different atmospheric systems dominating different parts of the Tibetan Plateau. The 7.5–8.5 ka peak (8 k event) in the PDF plot is dominant in Figures 5a–c (data from the Mu Us desert in northern China), suggesting a common driving force for this arid event in both the Tibetan Plateau and the Mu Us desert in Northern China. These sand accumulation events imply roughly synchronous environmental responses to global changes of corresponding global-scale arid events.

Acknowledgments

ZPL thanks the Alexander von Humboldt Foundation for a fellowship. Zhong He helped in collecting the luminescence data in the Mu Us desert. Field work was partly supported by the German Research Foundation (DFG KA 2713/1-1). Also supported by a CAS One-Hundred Talent Project granted to ZPL, and China NSF (40872119). We thank Ashok Singhvi, Bernd Wünnemann and two anonymous referees for very helpful comments.

Appendix A. Supplementary data

Supplementary data associated with this article can be found, in the online version, at doi:10.1016/j.yqres.2009.07.005.

References

Aitken, M.J., 1998. An Introduction to Optical Dating. Oxford University Press, Oxford. 262 pp.
Alley, R.B., Ágústsdóttir, A.M., 2005. The 8 k event: cause and consequences of a major Holocene abrupt climate change. Quaternary Science Reviews 24, 1123–1149.
An, Z.S., Kukla, G.J., Porter, S.C., Xiao, J., 1991. Magnetic susceptibility evidence of monsoon variation on the Loess Plateau of central China during the last 130,000 years. Quaternary Research 36, 29–36.
An, Z.S., Kutzbach, J.E., Prell, W.L., Porter, S.C., 2001. Evolution of Asian monsoons and phased uplift of the Himalaya-Tibetan plateau since Late Miocene times. Nature 411, 62–66.
Atlas of Tibet Plateau, 1990. Edited by the Institute of Geography, Chinese Academy of Sciences, Beijing (in Chinese).
Berger, A.L., 1978. Long-term variations of caloric insolation resulting from the Earth's orbital elements. Quaternary Reseasrch 9, 139–167.
Böhner, J., 1994. Circulation and representativeness of precipitation and air temperature in the southeast of the Qinghai-Xizang Plateau. GeoJournal 34, 55–66.
Bond, G., Kromer, B., Beer, J., Muscheler, R., Evans, M.N., Showers, W., Hoffmann, S., Rusty Lotti-Bond, R., Hajdas, I., Bonani, G., 2001. Persistent solar influence on North Atlantic climate during the Holocene. Science 294, 2130–2136.

Bøtter-Jensen, L., Bulur, E., Duller, G.A.T., Murray, A.S., 2000. Advances in luminescence instrumentation. Radiation Measurements 32, 523–528.
Bøtter-Jensen, L., McKeever, S.W.S, Wintle, A.G., 2003. Optically Stimulated Luminescence Dosimetry. Elsevier, Amsterdam.
Bryson, R.A., 1986. Airstream climatology of Asia. Proceedings of International Symposium on the Qinghai-Xizang Plateau and Mountain Meteorology. American Meteorological Society, Boston, MA, pp. 604–617.
Derbyshire, E., Shi, Y., Li, J., Zheng, B., Li, S., Wang, J., 1991. Quaternary glaciation of Tibet: the geological evidence. Quaternary Science Reviews 10, 485–510.
Ding, Z.L., Rutter, N., Han, J.T., Liu, T.S., 1992. A coupled environmental system formed at about 2.5 Ma in East Asia. Palaeogeography, Palaeoclimatology, Palaeoecology 94, 223–242.
Domrös, M., Peng, G., 1988. The Climate of China. Springer, Berlin.
Fan, Q.S., Lai, Z.P., Long, H., Sun, Y.J., Liu, X.J., in press. OSL chronology for lacustrine sediments recording high stands of Gahai Lake in Qaidam Basin, northeastern Qinghai-Tibetan Plateau. Quaternary Geochronology. doi:10.1016/j.quageo.2009.02.012.
Fang, X.M., 1995. The origin and provenance of the Malan loess along the eastern margin of the Qinghai–Xizang (Tibetan) Plateau and its adjacent area. Science in China (B) 38, 876–887.
Fang, X., Lü, L., Mason, J.A., Yang, S., An, Z., Li, J., 2003. Pedogenic response to millennial summer monsoon enhancements on the Tibetan Plateau. Quaternary International 106/107, 79–88.
Fielding, E., Isacks, B., Barazangi, M., Duncan, C., 1994. How flat is Tibet? Geology 22, 163–167.
Gasse, F., Fontes, J.Ch., Van Campo, E., WeiHolocene, K., 1996. Environmental changes in Bangong Co basin (Western Tibet). Part 4: discussion and conclusions. Palaeogeography, Palaeoclimatology, Palaeoecology 120, 79–92.
Herzschuh, U., Winter, K., Wünnemann, B., Li, S., 2006. A general cooling trend on the central Tibetan Plateau throughout the Holocene recorded by the Lake Zigetang pollen spectra. Quaternary International 154/155, 113–121.
Kaiser, K., 2007. Soils and terrestrial sediments as indicators of Holocene environmental changes on the Tibetan Plateau. Habilitation thesis, Faculty of Geography, University of Marburg, 192 pp.
Kaiser, K., Lai, Z.P., Schneider, B., Reudenbach, C., Miehe, G., Brückner, H., 2009a. Stratigraphy and palaeoenvironmental implications of Pleistocene and Holocene aeolian sediments in the Lhasa area, southern Tibet (China). Palaeogeography, Palaeoclimatology, Palaeoecology 271, 329–342.
Kaiser, K., Opgenoorth, L., Schoch, W.H., Miehe, G., 2009b. Charcoal and fossil wood from palaeosols, sediments and artificial structures indicating Late Holocene woodland decline in southern Tibet. Quaternary Science Reviews 28, 1539–1554.
Kaiser, K., Lai, Z.-P., Schneider, B., Schoch, W.H., Shen, X.H., Miehe, G., Brückner, H., 2009c. Sediment sequences and paleosols in the Kyichu Valley, southern Tibet (China), indicating Late Quaternary environmental changes. The Island Arc 18 (3), 404–427.
Kaiser, K., Lai, Z.P., Schneider, B., Junge, F.W., 2009d. Late Pleistocene genesis of the middle Yarlung Zhangbo Valley, southern Tibet (China), as deduced by sedimentological and luminescence data. Quaternary Geochronology, doi:10.1016/j.quageo.2009.01.005.
Kuhle, M., 1998. Reconstruction of the 2.4 million km^2 late Pleistocene ice sheet on the Tibetan Plateau and its impact on the global climate. Quaternary International 45 (/46), 71–108.
Kuhle, M., 2005. Glacial geomorphology and ice ages in Tibet and the surrounding mountains. The Island Arc 14, 346–367.
Kukla, G., An, Z., 1989. Loess stratigraphy in central China. Palaeogeography, Palaeoclimatology, Palaeoecology 72, 203–225.
Lamb, H.F., Gasse, F., Benkaddour, A., Hamouti, N., Kaars, S., Perkins, W.T., Pearce, N.J., Roberts, C.N., 1995. Relation between century-scale Holocene arid intervals in tropical and temperate zones. Nature 373, 134–137.
Lai, Z.P., in press. Chronology and the upper dating limit for loess samples from Luochuan section in the Chinese Loess Plateau using quartz OSL SAR protocol. Journal of Asian Earth Sciences. doi:10.1016/j.seaes.2009.08.003.
Lai, Z.P., Brückner, H., 2008. Effects of feldspar contamination on equivalent dose and the shape of growth curve for OSL of silt-sized quartz extracted from Chinese loess. Geochronometria 30, 49–53.
Lai, Z.P., Wintle, A.G., 2006. Locating the boundary between the Pleistocene and the Holocene in Chinese loess using luminescence. The Holocene 16, 893–899.
Lai, Z.P., Singhvi, A.K., Chen, H.Z., Zhou, W.J., 1999. Luminescence chronology of Holocene sediments from Taipingchuan in loess/desert transitional zone, China and its implication. Man and Environment 14, 91–97.
Lai, Z.P., Wintle, A.G., Thomas, D.S.G., 2007. Rates of dust deposition between 50 ka and 20 ka revealed by OSL dating at Yuanbao on the Chinese Loess Plateau. Palaeogeography, Palaeoclimatology, Palaeoecology 248, 431–439.
Lai, Z.P., Zöller, L., Fuchs, M., Brückner, H., 2008a. Alpha efficiency determination for OSL of quartz extracted from Chinese loess. Radiation Measurements 43, 767–770.
Lai, Z.P., Brückner, H., Zöller, L., Fülling, A., 2008b. Effects of thermal treatment on the growth curve shape for OSL of quartz extracted from Chinese loess. Radiation Measurements 43, 763–766.
Lancaster, N., 1990. Palaeoclimatic evidence from sand seas. Palaeogeography, Palaeoclimatology, Palaeoecology 76, 279–290.
Lancaster, N., 2008. Desert dune dynamics and development: insights from luminescence dating. Boreas 37, 559–573.
Lehmkuhl, F., 1997. The spatial distribution of loess and loess-like sediments in the mountain areas of Central and High Asia. Zeitschrift für Geomorphologie Supplement 111, 97–116.
Lehmkuhl, F., Klinge, M., Rees-Jones, J., Rhodes, E.J., 2000. Late Quaternary eolian sedimentation in central and south-eastern Tibet. Quaternary International 68-71, 117–132.
Lehmkuhl, F., Klinge, M., Lang, A., 2002. Late Quaternary glacier advances, lake level fluctuations and aeolian sedimentation in Southern Tibet. Zeitschrift für Geomorphologie Supplement 126, 183–218.
Li, S.H., Sun, J.M., Zhao, H., 2002. Optical dating of dune sands in the northeastern deserts of China. Palaeogeography, Palaeoclimatology, Palaeoecology 181, 419–429.
Li, X.Z., Yi, C.L., Chen, F.H., Yao, T.D., Li, X., 2006. Formation of proglacial dunes in front of the Puruogangri Icefield in the central Qinghai-Tibet Plateau: implications for reconstructing paleoenvironmental changes since the Lateglacial. Quaternary International 154/155, 122–127.
Liu, T.S., 1985. Loess and the Environment. China Ocean Press, Beijing. 251 pp.
Liu, X.Q., Shen, J., Wang, S.M., Yang, X.D., Tong, G.B., Zhang, E.L., 2002. A 16000-year pollen record of Qinghai Lake and its paleoclimate and paleoenvironment. Chinese Science Bulletin 47, 1931–1936.
Liu, X.J., Lai, Z.P., Long, H., Fan, Q.S., Sun, Y.J., in press. Timing for high lake level of Qinghai lake in the Qinghai-Tibet Plateau based on quartz optically stimulated luminescence dating. Quaternary Geochronology. doi:10.1016/j.quageo.2009.03.010.
Long, H., Lai, Z.P., Fan, Q.S., Sun, Y.J., Liu, X.J., in press. Applicability of a quartz OSL standardised growth curve for De determination up to 400 Gy for lacustrine sediments from the Qaidam Basin of the Qinghai-Tibetan Plateau. Quaternary Geochronology. doi:10.1016/j.quageo.2009.05.005.
Lu, H.Y., Wang, X.Y., Ma, H.Z., Tan, H.B., Vandenberghe, J., Miao, X.D., Li, Z., Sun, Y.B., An, Z.S., Cao, G.C., 2004. The plateau monsoon variation during the past 130 kyr revealed by loess deposit at northeast Qinghai-Tibet (China). Global and Planetary Change 41, 207–214.
Lu, H.Y., Miao, X.D., Zhou, Y.L., Joseph, M., James, S., Zhang, J.F., Zhou, L.P., Yi, S.W., 2005. Late Quaternary Aeolian activity in the Mu Us and Otindag dune fields (North China) and lagged response to insolation forcing. Geophysical Research Letters 32, L21716.
Madsen, D.B., Ma, H.Z., Rhode, D., Brantingham, P.J., Forman, S.T., 2008. Age constraints on the late Quaternary evolution of Qinghai Lake, Tibetan Plateau. Quaternary Research 69, 316–325.
Martinson, D.G., Pisias, N.G., Hays, J.D., Imbrie, J., Moore, T.C., Shackleton, N.J., 1987. Age dating and the Orbital Theory of the Ice Ages: Development of a High-Resolution 0 to 300,000-Year Chronostratigraphy 27, 1–29.
McFarlane, M.J., Eckardt, F.D., Ringrose, S., Coetzee, S.H., Kuhn, J.R., 2005. Degradation of linear dunes in Northwest Ngamiland, Botswana and the implications for luminescence dating of periods of aridity. Quaternary International 135, 83–90.
Miehe, G., Winiger, M., Böhner, J., Zhang, Y.L., 2001. The climatic diagram map of High Asia. Purpose and concepts. Erdkunde 55, 94–97.
Miehe, G., Miehe, S., Schlütz, F., Kaiser, K., La, Duo, 2006. Palaeoecological and experimental evidence of former forests and woodlands in the treeless desert pastures of Southern Tibet (Lhasa, A.R. Xizang, China). Palaeogeography, Palaeoclimatology, Palaeoecology 242, 54–67.
Murray, A.S., Wintle, A.G., 2000. Luminescence dating of quartz using an improved single-aliquot regenerative-dose protocol. Radiation Measurements 32, 57–73.
Nanson, G.C., Chen, X.Y., Price, D.M., 1992. Lateral migration, thermoluminescence chronology and color variation of longitudinal dunes near Birdsville in the Simpson Desert, Central Australia. Earth Surface Processes and Landforms 17, 807–819.
Ou, X.J., Lai, Z.P., Xu, L.B., Long, H., He, Z., Fan, Q.S., Zhou, S.Z., in press. Potential of quartz OSL dating on morainic deposits from eastern Tibetan Plateau using SAR protocol. Quaternary Geochronology. doi:10.1016/j.quageo.2009.02.004.
Owen, L.A., Finkel, R.C., Caffee, M.W., 2002. A note on the extent of glaciation in the Himalaya during the global Last Glacial Maximum. Quaternary Science Reviews 21, 147–157.
Owen, L.A., Finkel, R.C., Ma, H.Z., Barnard, P.L., 2006. Late Quaternary landscape evolution in the Kunlun Mountains and Qaidam Basin, Northern Tibet: a framework for examining the links between glaciation, lake level changes and alluvial fan formation. Quaternary International 154/155, 73–86.
Péwé, T.L., Liu, T.S., Slatt, R.M., Li, B.Y., 1995. Origin and character of loesslike silt in the southern Qinghai-Xizang (Tibet) Plateau, China. US Geological Survey Professional Paper 1549, 1–55.
Porter, S.C., An, Z.S., 1995. Correlation between climate events in the North Atlantic and China during the last glaciation. Nature 375, 305–308.
Porter, S.C., Zhou, W.J., 2006. Synchronism of Holocene East Asian monsoon variations and North Atlantic drift-ice tracers. Quaternary Research 65, 443–449.
Porter, S.C., Singhvi, A., Zhisheng, A., Zhongping, L., 2001. Luminescence age and palaeoenvironmental implications of a late Pleistocene ground wedge on the Northeastern Tibetan Plateau. Permafrost and Periglacial Processes 12, 203–210.
Prescott, J.R., Hutton, J.T., 1994. Cosmic ray contributions to dose rates for luminescence and ESR dating: large depths and long-term time variations. Radiation Measurements 23, 497–500.
Roberts, H.M., Muhs, D.R., Wintle, A.G., Duller, G.A.T., Bettis III, E.A., 2003. Unprecedented last-glacial mass accumulation rates determined by luminescence dating of loess from western Nebraska. Quaternary Research 59, 411–419.
Ruddimann, W.F., Kutzbach, J.E., 1989. Forcing of Late Cenozoic Northern Hemisphere climate by plateau uplift in southern Asia and the America west. Journal of Geophysical Research 94, 18,409–18,427.
Shen, J., Liu, X.Q., Wang, S.M., Matsumoto, R., 2005. Palaeoclimatic changes in the Qinghai Lake area during the last 18,000 years. Quaternary International 136, 131–140.

Shi, Y., Zheng, B., Li, S., 1992. Last glaciation and maximum glaciation in the Qinghai-Xizang (Tibet) Plateau: a controversy to M. Kuhle's ice sheet hypothesis. Zeitschrift für Geomorphologie Supplement 84, 19–35.
Singhvi, A.K., Porat, N., 2008. Impact of luminescence dating on geomorphological and palaeoclimate research in drylands. Boreas 37, 536–558.
Singhvi, A.K., Bronger, A., Sauer, W., Pant, R.K., 1989. Thermoluminescence dating of loess/palaeosol sequences in the Carpathian Basin (east Central Europe): a suggestion for a revised chronology. Chemical Geology (Isotopic Geosciences Section) 73, 307–317.
Singhvi, A.K., Bluszcz, A., Bateman, M.D., Rao, M.S., 2001. Luminescence dating of loess-palaeosol sequences and coversands: methodological aspects and palaeoclimatic implications. Earth-Science Reviews 54, 193–211.
Sun, J.M., Li, S.H., Han, P., Chen, Y.Y., 2006. Holocene environmental changes in central Inner Mongolia, based on single-aliquot-quartz optical dating and multi-proxy study of dune sands. Palaeogeography, Palaeoclimatology, Palaeoecology 233, 51–62.
Sun, J.M., Li, S.H., Muhs, D.R., Li, B., 2007. Loess sedimentation in Tibet: provenance, processes, and link with Quaternary glaciations. Quaternary Science Reviews 26, 2265–2280.
Sun, Y.J., Lai, Z.P., Long, H., Liu, X.J., Fan, Q.S., in press. Quartz OSL dating of archaeological sites in Xiao Qaidam Lake of the NE Qinghai-Tibetan Plateau and its implication for palaeoenvironmental changes. Quaternary Geochronology. doi:10.1016/j.quageo.2009.02.013.
Telfer, M.W., Thomas, D.S.G., 2007. Late Quaternary linear dune accumulation and chronostratigraphy of the southwestern Kalahari: implications for aeolian palaeoclimatic reconstructions and predictions of future dynamics. Quaternary Science Reviews 26, 2617–2630.
Thompson, L.G., Mosley-Thompson, E., Davis, M.E., Bolzan, J.F., Dai, J., Yao, T., Gundestrup, N., Wu, X., Klein, L., Xie, Z., 1989. Holocene-Late Pleistocene climatic ice core records from Qinghai-Tibetan Plateau. Science 246, 474–477.
Thompson, L.G., Yao, T., Davis, M.E., Henderson, K.A., Mosley-Thompson, E., Lin, P.-N., Beer, J., Synal, H.-A., Cole-Dai, J., Bolzan, J.F., 1997. Tropical climate instability: the last glacial cycle from a Qinghai-Tibetan ice core. Science 276, 1821–1825.
van Campo, E., Gasse, F., 1993. Pollen- and diatom-inferred climatic and hydrological changes in Sumxi Co Basin (Western Tibet) since 13,000 yr B.P. Quaternary Research 39, 300–313.
Wang, Y.J., Cheng, H., Edwards, R.L., Kong, X.G., Shao, X.H., Chen, S.T., Wu, J.Y., Jiang, X.Y., Wang, X.F., An, Z.S., 2008. Millennial- and orbital-scale changes in the East Asian monsoon over the past 224,000 years. Nature 451, 1090–1092.
Wanner, H., Beer, J., Buetikofer, J., Crowley, T.J., Cubasch, U., Flueckiger, J., Goosse, H., Grosjean, M., Joos, F., Kaplan, J.O., Kuettel, M., Mueller, S.A., Prentice, C., Solomina, O., Stocker, T.F., Tarasov, P., Wagner, M., Widmannm, M., 2008. Mid- to Late Holocene climate change: an overview. Quaternary Science Reviews 27, 1791–1828.
Wintle, A.G., Murray, A.S., 2006. A review of quartz optically stimulated luminescence characteristics and their relevance in single-aliquot regeneration dating protocols. Radiation Measurements 41, 369–391.
Wu, Y.H., Lücke, A., Jin, Z.D., Wang, S.M., Schleser, G.H., Battarbee, R.W., Xia, W.L., 2006. Holocene climate development on the central Tibetan Plateau: a sedimentary record from Cuoe Lake. Palaeogeography, Palaeoclimatology, Palaeoecology 234, 328–340.
Yao, T.D., Thompson, L.G., Shi, Y.F., Qin, D.H., Jiao, K.Q., Yang, Z.H., Tian, L.D., Thompson, E.M., 1997. Climate variation since the last interglaciation recorded in the Guliya ice core. Science in China (Ser. D) 40 (6), 662–668.
Ye, D.Z., Gao, Y.X., 1988. Meteorology of the Tibetan Plateau. Science Press, Beijing. 1988, 420 pp. (in Chinese).
Zheng, B.X., Rutter, N., 1998. On the problem of Quaternary glaciations, and the extent and patterns of Pleistocene ice cover in the Qinghai-Xizang (Tibet) Plateau. Quaternary International 45/46, 109–122.
Zhou, S., Li, J., 1998. The sequence of Quaternary glaciation in the Bayan Har Mountains. Quaternary International 45/46, 135–142.